Semi-analytical design methodology for large scale metal–insulator–metal waveguide networks

2014 J. Opt. 16 065007

(http://iopscience.iop.org/2040-8986/16/6/065007)

IOP Publishing Journal of Optics
J. Opt. **16** (2014) 065007 (11pp) doi:10.1088/2040-8978/16/6/065007

Semi-analytical design methodology for large scale metal–insulator–metal waveguide networks

Mohamed A Swillam[1] **and Amr S Helmy**[2]

[1] Department of Physics, The American University in Cairo, New Cairo, 11835, Egypt
[2] The Edward S. Rogers Sr. Department of Electrical and Computer Engineering, University of Toronto, 10 King's College Road, Toronto, Ontario MSS 3G4, Canada

E-mail: m.swillam@aucegypt.edu

Received 29 January 2014, revised 21 March 2014
Accepted for publication 28 March 2014
Published 29 May 2014

Abstract

A semi-analytical approach for efficient modelling of large scale networks of plasmonic metal–insulator–metal waveguides is proposed and its efficacy is assessed. A simple model for a wide range of waveguide junction configurations that can be obtained using waveguide impedance is utilized. This efficient and accurate model enables full analysis of a complete network of plasmonic waveguides without the need for any full-wave analysis. The proposed approach is computationally efficient and enables rapid design and optimization cycles using these networks. The results obtained using our approach match those obtained with finite difference time domain simulations. Several example structures have been analyzed using this approach, where their performance has been optimized through the multivariable optimization afforded by the technique reported here.

Keywords: plasmonic waveguides, integrated photonics, filters

1. Introduction

The unique ability of plasmonic waveguides to guide light in subwavelength dimensions can empower various attractive applications. The applications include biomedical sensing [1, 2], optical interconnects [3], and surface enhanced Raman scattering [4]. The ability to stack large number of waveguides on nanometer scale with negligible cross-talk is an important characteristic that provides an optimal solution for large dense integration of photonic devices. Various waveguide structures have been proposed for such applications. Among the different waveguide configurations, metal–insulator–metal (MIM) and insulator–metal–insulator (IMI) were widely used due to the relative ease of their analysis and fabrication. IMI waveguide is considered as suitable candidate for surface sensing based on long range SPP mode [5]. However, this configuration does not provide suitable confinement for interconnects or dense on-chip integration.

On the other hand, the MIM waveguide configuration is a suitable candidate for various on-chip applications including sensing and interconnects [6, 7].

Plasmonic slot waveguide (PSW) represents a 3D practical realization of the MIM configuration. This waveguide is one of the most suitable candidates for on chip device applications as the mode is in the nanometer scale. The slot waveguide configuration can also be exploited as a fluidic channel for on-chip bio-sensing applications.

PSWs and MIM have been utilized for different devices including power splitting [8], filtering [9], switching, modulation, multiplexing and de-multiplexing [8, 10]. These waveguides suffer from high propagation losses, which scale up with increasing the confinement. Thus, for this useful utilization any functionality sought should be obtained in few micrometers to mitigate the shortcomings of the excessive propagation losses. In addition, in and out coupling approaches for this class of waveguide from conventional dielectric waveguides are very challenging due to the mismatch in the modal field profile and

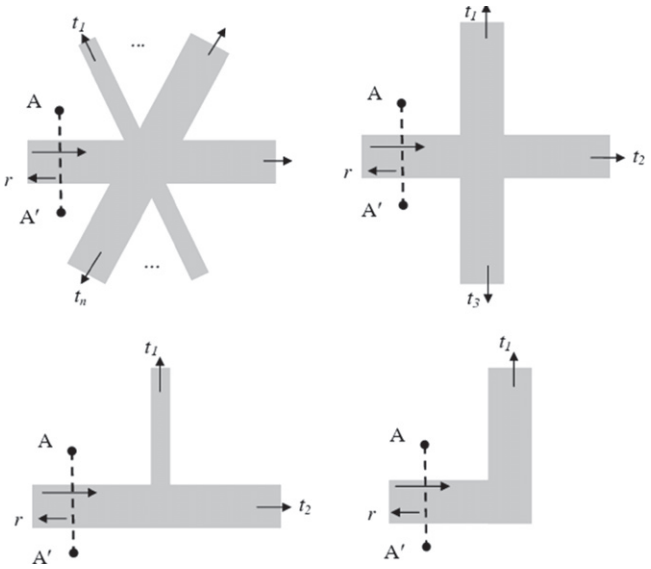

Figure 1. Schematics of different plasmonic junctions using PSW.

also due to the difference in the modal size. Recently a simple, efficient, wideband, and nonresonant coupling mechanism and have been demonstrated to solve the coupling dilemma [11, 12].

Having achieved efficient in and out coupling to and from PSWs, they are ready to be utilized in various applications. For example, the ability to create low loss 90° bends [13] and T and X junctions with good coupling to all orthogonal branches are unique features for MIM and PSW. These features can be exploited to create a network (mesh) of MIM waveguides, which can be exploited in different applications. For example, these networks can be readily exploited for designing wideband filters [14], and band reject notch filter response [15].

However, modelling of these plasmonic networks is highly demanding due to the fine mesh required to accurately predict the device response. As a result, the computational resources required for any full vectorial electromagnetic solver used to model such networks are significant. This of course impedes the design process and reduces the ability to explore novel architectures using these networks. Some attempts for modelling limited scale networks have been recently proposed [16]. However, these attempts still rely on the finite difference time domain (FDTD) to predict the optical field characteristics at each junction. This provides limited saving in the computational resources and also in reducing the complexity of the optimization process. Thus, a novel and efficient modelling scheme that takes into account the unique features of the plasmonic networks and is able to predict the performance of large plasmonic networks is still lacking.

Recently, a simple impedance model for the T and X junctions has been proposed [14, 15, 17]. This model is used to obtain analytical closed form expressions of various responses of functional devices using MIM configuration. Even though the model is simple and straightforward, it provides accurate results compared to FDTD. The model is mainly based on estimating the transmission and the reflection of each junction using a simple but effective impedance model. The model is also applicable for PSWs if the thickness of the metal is larger than the width of the slot [18]. For a network of MIM waveguides or PSWs that contains few junctions, the impedance model can be exploited using the scattering matrix method to develop an analytical closed form expression for the reflection and the transmission from each port of the network. The approach has been validated for different structures with few junctions demonstrating very good accuracy and negligible computational effort [15, 17]. However, for network structures with large number of junctions, this approach produces complex closed form equations that provide less insight into the design in comparison to the case with only a few junctions. Thus, the aforementioned approach is mainly suitable for networks with limited number of junctions.

For structures with relatively large number of junctions, the FDTD requires tremendous computational resources to be able to estimate the output from each port. For such large networks, the number of design variables (which can be branche dimensions and core refractive indices) become exceedingly large. The ability to optimize these variables to attain a certain performance or function is inhibited by the excessive computational resources needed. On the other hand, the analytical results obtained from the impedance model provide good estimates for the reflection and transmission of each junction in this large network and thus can be used to alleviate the computational resources needed for analysis while maintaining the numerical nature of the analysis. Thus, it is of prime importance to analyze these networks with relatively large scale using an approach that is efficient and has good accuracy.

In this paper, we propose and analyze a general and efficient approach that is capable of modelling any large scale network of PSWs without the need of any electromagnetic solver. This approach makes use of the accurate estimates of the junctions reflection and transmission coefficients that can be obtained for each junction using the impedance model. It also alleviates the need for obtaining a closed form for the final response at each port. Thus, this approach can be considered as a semi-analytical version of the closed form one proposed in [15, 17]. This approach can handle any type of MIM waveguides. The model is also applicable for PSWs if the thickness of the metal is larger than the width of the slot [18]. In addition it is very simple to implement and allow for fast optimization cycle for the response of each port in these networks. Also in this work we exploited this model to investigate and analyze some network topologies for useful functions such as filter and modulator responses. These network based devices are distinctive and usher in a new route of using the MIM/PSW networks.

We start by analyzing the plasmonic junction and the impedance model used to model these junctions in section 2. In section 3, the proposed model is described and the implementation details are presented. An efficient approach for sensitivity calculation using this approach is also given in section 4. The various examples are presented to compare the accuracy of the model against FDTD in section 5. Finally, the conclusion is given in section 6.

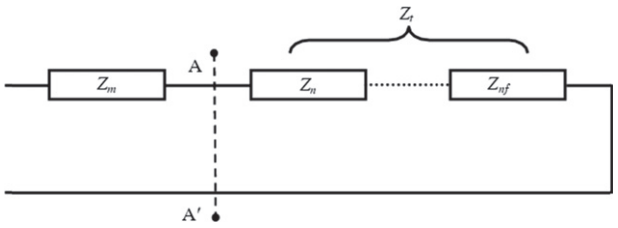

Figure 2. The equivalent circuit of plasmonic junctions using PSW.

2. Junction analysis using an impedance model

Accurate and simple modelling of different junctions is essential for any given network topology that is composed of these junctions. Most of the current models for these junctions are based on full wave electromagnetic simulation using the FDTD method [19, 20]. However, the utilization of the FDTD simulation to obtain the output for each junction is inefficient, especially for networks with complex junction shapes and large feature dimensions. In addition, it also does not allow for physical understanding of the junction behavior, which is essential for obtaining the required functionality.

In this section, a simple model for various junctions is discussed in details. These junctions contain orthogonally connected waveguides as shown in figure 1. Unlike conventional dielectric photonic waveguides, PSWs can have efficient coupling to orthogonal waveguide. This phenomenon is analogous to metallic waveguides operating at microwave frequencies, in which case the T junctions behave well with 90 degrees bends. Thus, using coupled mode theory, for example to calculate the coupling coefficients is cumbersome and will increase the complexity of the model. As such, the waveguide impedance is exploited instead to define the amount of the power coupled or reflected at each port of the junction. This model is simple and efficient and has comparable accuracy to results obtained using FDTD [14, 15, 17].

The model is based on creating a transmission line equivalent model for each PSW section. At the junction the loading of each waveguide is distributed according to its impedance as shown in the equivalent circuit model in figure 2. The power reflected from the input waveguide and the power transmitted to all the output ports are calculated as follows.

$$r_m = \left| \frac{Z_t - Z_m}{Z_t + Z_m} \right| . \, e^{-2\gamma l_m}, \tag{1}$$

and

$$t_{nm} = \left| \sqrt{\frac{Z_n}{Z_t}} \times \frac{2\sqrt{Z_m Z_t}}{(Z_m + Z_t)} \right| . \, e^{-\gamma(l_{in}+l_n)} \tag{2}$$

where

$$Z_m(\omega, d) = \frac{\beta_{PSW}(\omega, d)\, d}{\omega \varepsilon(\omega)} \tag{3}$$

where Z_m and Z_n are the waveguide impedance of the input port section and the loading sections, respectively as shown in figure 2. β_{PSW} is the propagation constant of the PSW. More

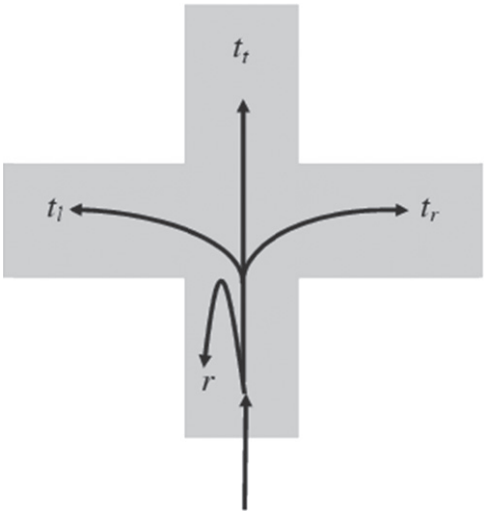

Figure 3. Schematics of the X junction.

accurate calculation of the plasmonic slot impedance has been recently presented and can be easily incorporated in our model [21]. The reflection and transmission from each port of an X junction are shown in figure 3 as an example. The wave propagation behavior obtained from this model match well with those obtained from FDTD as shown in figure 4. For these simulations, air is used as the insulating media between the metals for modeling an asymmetric X junction. For this junction, the vertical arms have a width of 100 nm and the horizontal arms of 50 nm width The metal used is adopted from the experimental data in [22] by direct fitting to multi-coefficient FDTD model in [23]. The same source for the values of the permittivity of the metal are also utilized for our model. Two point fitting technique is utilized to estimate the values in between the measured data. This model produces accurate results for PSW for widths $<\lambda/6$ [17].

3. Semi-analytical approach for modeling PSW network

This proposed approach is based on transforming the field output from each junction and then connecting it to the neighboring junctions sequentially until the field reaches the output ports of the network. The concept of scattering junctions has been utilized for microwave structures [24]. However, this concept is not widely utilized in photonic devices due to the fact that obtaining the scattering parameters of any optical junction is carried out through full wave electromagnetic simulations, which severely limit the advantages of using this approach [16, 25]. The simple impendence models of MIM-based junctions allows for obtaining the scattering parameters for each junction analytically without the need of any full wave simulation. The fact that MIM and PSW behave similar to microwave metallic waveguides more than photonic waveguides triggers the interest in utilizing the scattering method for their analysis. However, direct application of such techniques does not readily yield accurate results. This is due to the need for carful understanding and handling of MIM and

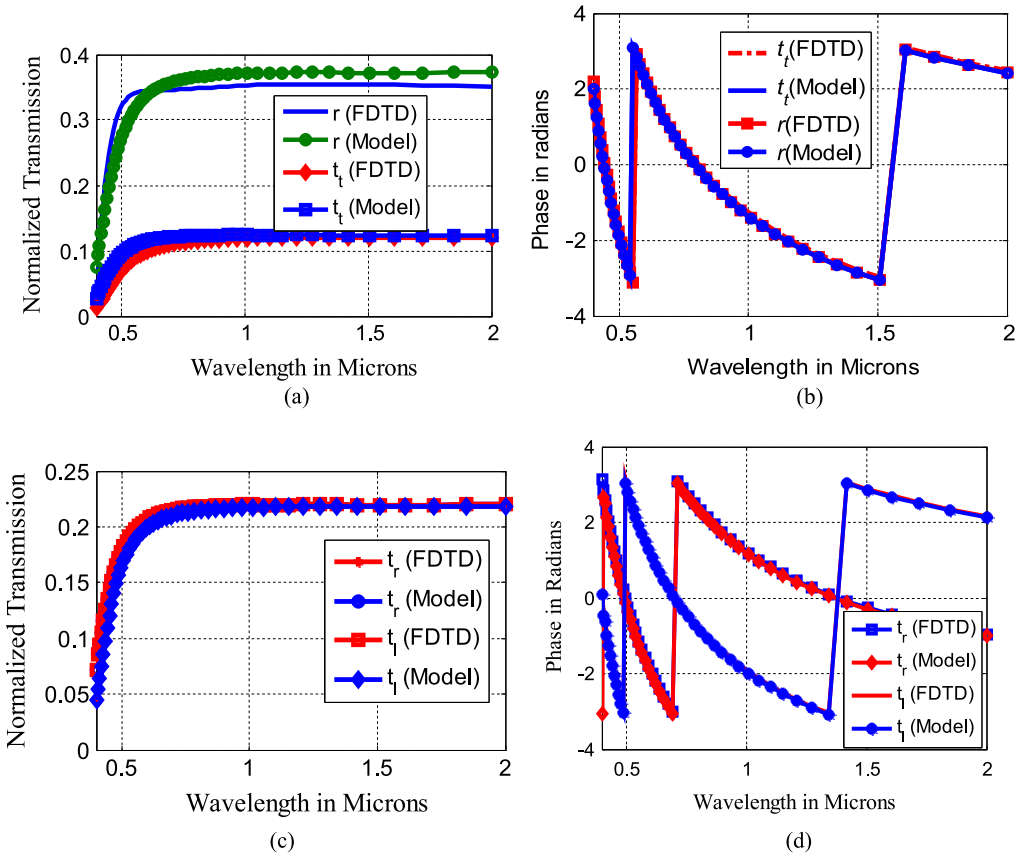

Figure 4. Normalized transmission for an asymmetric silver X junction of 50 nm horizontal arms for both the through and reflection power shown in (a) and 100 nm vertical arms for both the left and right arms shown in (b) as well as the phase in the horizontal arms (c) and the vertical arms (d).

PSW-based junctions that have distinct properties from their microwave counterparts. For example the *even* and *odd* mode symmetry of the transverse electric field components in these waveguides plays an important role in the phase information at each port of the T and X junctions. For example, the two longitudinal arms have in phase field while the orthogonal arm is out phase. More details about the exact junction modeling are given hereafter. Thus, the implementation details, parameter and coefficients definitions need to be specific to a given PSW and MIM plasmonic waveguide case in comparison to the generic microwave approach.

3.1. Junction modelling

The initial stage is accounting for the scattering at each individual junction. At this step the field injected inside the junction is split into the different arms as shown in figure 3. The magnitude and phase of the splitting ratio is obtained by expressions (1) and (2).

The field at each arm of the junction due to the scattering process can be obtained using the reciprocity theorem as follows;

$$\begin{aligned} e_1^o &= r_1 e_1^i + t_1^l e_2^i + t_1^t e_3^i + t_1^r e_4^i \\ e_2^o &= t_2^r e_1^i + r_2 e_2^i + t_2^l e_3^i + t_2^t e_4^i \\ e_3^o &= t_3^t e_1^i + t_3^r e_2^i + r_3 e_3^i + t_3^l e_4^i \\ e_4^o &= t_4^l e_1^i + t_4^t e_2^i + t_4^r e_3^i + r_4 e_4^i \end{aligned} \quad (4)$$

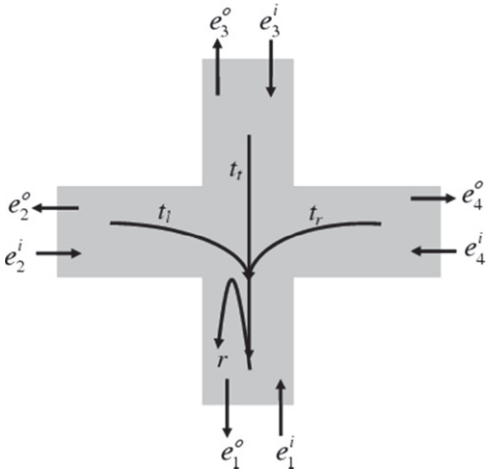

Figure 5. The transmission and reflection coefficients at each port of the plasmonic junction.

This process occurs at each junction. Where e_n^i and e_n^o are the input and output fields from nth ports of the X junction, respectively as defined in figure 5. The junction can include any number of ports. For example, if the junction is T shape, three ports take part, then the equations in (4) can be modified to assume that the all the power in port 4 which is now removed port is totally reflected and the power transmitted through this port is zero.

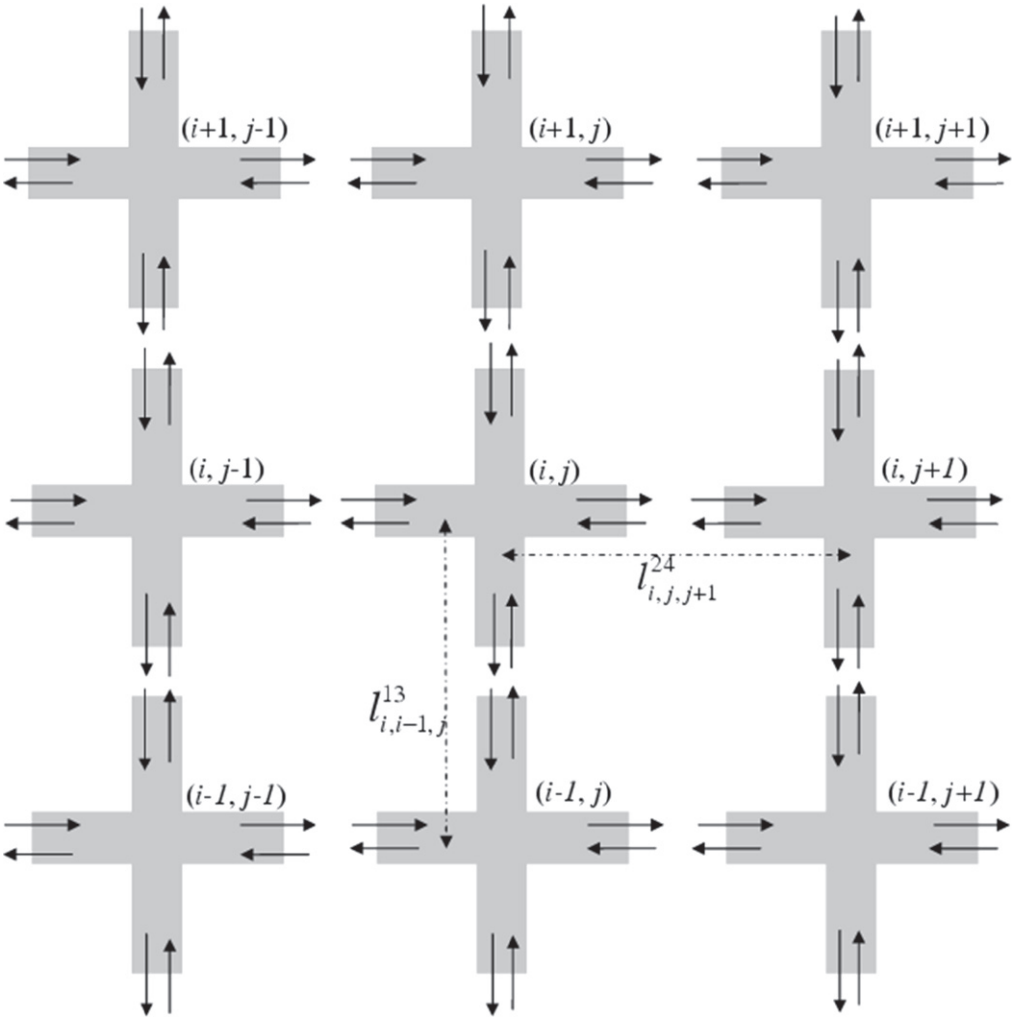

Figure 6. Schematic diagram of a general plasmonic network using PSWs.

3.2. Network modelling

In order to model the network behavior, the output from each junction is connected to the adjacent junctions through a propagation operator P. For example, the output field from port 3 in junction $(i-1, j)$ is directly connected as the input of port 1 in junction i, j as shown in figure 6. This connection process is mathematically described as follows

$$e_1^i\Big|_{i,j} = P^{13}_{i,i-1}\ e_3^o\Big|_{i-1,j} \tag{5}$$

where i and j represent the vertical and horizontal indices of the junction and $e_1^i\Big|_{i,j}$ is the input field of port 1 of this junction. The operator $P^{13}_{i,i-1,j}$ is the propagation operator from port 3 of junction $(i-1, j)$ to port 1 of junction (i, j) and is given by

$$P^{13}_{i,i-1,j} = \frac{e^{-\gamma^{13}_{i,i-1,j} l^{13}_{i,i-1,j}}}{1 - r_{1,i,j} r_{3,i-1,j} e^{-2\gamma^{13}_{i,i-1,j} l^{13}_{i,i-1,j}}} \tag{6}$$

where $\gamma^{13}_{i,i-1,j}$, and $l^{13}_{i,i-1,j}$ are the complex propagation constant and the length of the vertical waveguide between junction (i, j) and $(i-1, j)$, respectively. This operator includes the phase shift due to the propagation as well as the multiple internal reflections between the two junction interfaces. This operator assumes that the power transfer between junctions takes place mainly through the fundamental mode inside the waveguide connecting these junctions. This assumption is valid only if the effect of the scattering at each junction is ignored. This entails that there needs to be a minimum distance between the junctions of $\sim\lambda_n/6$ for this assumption to be valid.

3.3. System of equations for a network

By using the connection equations and by substituting the output field from each port with its scattered input field using the scattering equation, a system of equations can be constructed as a function of the incident fields only. For example, by substituting (4) into (5) we can write the following equation

$$0 = -e_1^i\Big|_{i,j} + P^1_{i,i-1} \times \left(t_3^t\ e_1^i\Big|_{i-1,j} + t_3^r\ e_2^i\Big|_{i-1,j} + r_3 e_3^i\Big|_{i-1,j} + t_3^l e_4^i\Big|_{i-1,j}\right) \tag{7}$$

Similar approach is applied for all the junctions connecting all the ports of the network. This will result in a

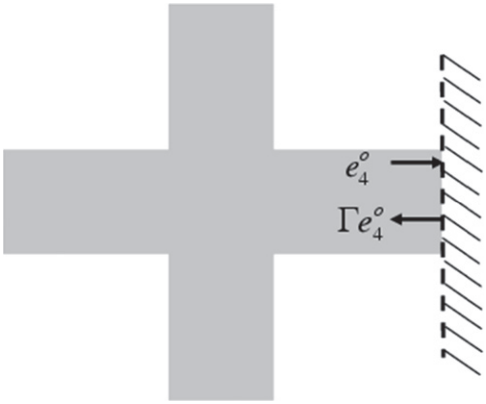

Figure 7. The schematic of a terminated junction.

system with $4n_xn_y$ equations which can be written as

$$\mathbf{A}E_i = E_s \tag{8}$$

where E_i is the input electric field vector of the four ports of all the junctions in the network. This vector is organized as follows

$$E_i = \left[e^i_{1,1,1} \;\; e^i_{2,1,1} \;\; e^i_{3,1,1} \;\; e^i_{4,1,1} \cdots \right. \\ \left. e^i_{1,nx,ny} \;\; e^i_{2,nx,ny} \;\; e^i_{3,nx,ny} \;\; e^i_{4,nx,ny} \right]^T \tag{9}$$

The length of this vector is $4n_xn_y$, where n_x and n_y are the number of junctions in the vertical and horizontal direction, respectively. E_s is the excitation of the network's port and has nonzero values only for the elements corresponding to the excited ports. At these elements a value of 1 is inserted in this vector with a minimum of one port excitation. The matrix **A** is the network matrix which contains the transmission and reflection coefficients as briefly descried in (7).

The reflection from boundaries modifies the connection step of the boundary junctions. For example for metallic boundary as shown in figure 7, the connection step is given as

$$e^i_4\big|_{i,j} = \Gamma_b \; e^o_4\big|_{i,j} \tag{10}$$

And hence the system equation for this junction is given as

$$e^i_4\big|_{i,j} = \Gamma_b \left(t^l_4 e^i_1\big|_{i,j} + t^t_4 e^i_2\big|_{i,j} + t^r_4 e^i_3\big|_{i,j} + r_4 e^i_4\big|_{i,j} \right) \tag{11}$$

The value of the reflection coefficient is crucial and depends on the boundary type. For example, for metallic boundaries, a perfect metal may be considered $(\Gamma_b = -1)$. However, more accurate results can be obtained by using a modified reflection coefficient by assuming real metal at optical frequencies [26]. This coefficient takes into account the metal/dielectric material system dispersion which can be given by

$$\Gamma(f) = \frac{\sqrt{\varepsilon_m(f)} - \sqrt{\varepsilon_d(f)}}{\sqrt{\varepsilon_d(f)} + \sqrt{\varepsilon_m(f)}} \tag{12}$$

Partial reflection can occur at an inner junction of the PSW waveguide which is connected to one of its port if two different materials are used. For example, inserting a dielectric material inside the slot of section of the waveguide will

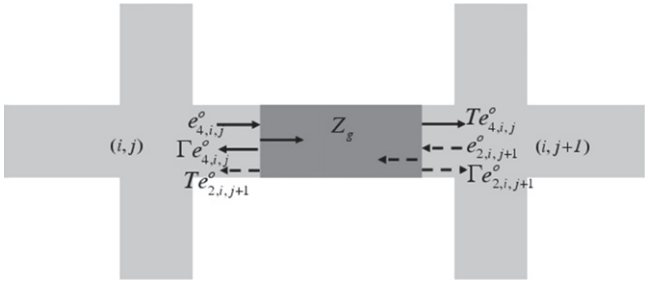

Figure 8. The reflection and transmission coefficients between two adjacent junctions.

create a partial reflection at each interface as shown in figure 8. This will require a modification of the connection equation as given below

$$e^i_4\big|_{i,j} = \Gamma^{24}_{j,j+1} \; e^o_4\big|_{i,j} + T^{24}_{j,j-1} \; e^o_2\big|_{j,j+1} \tag{13}$$

where

$$\Gamma = \frac{\rho_1 + \rho_2 e^{-2\gamma_i l_i}}{1 + \rho_1\rho_2 e^{-2\gamma_i l_i}}, \tag{14}$$

and

$$T = \frac{\tau_1\tau_2 e^{-\gamma_i l_{di}}}{1 + \rho_1\rho_2 e^{-2\gamma_i l_{di}}} \tag{15}$$

The Fresnel reflection coefficient in (14) is given by

$$\rho_1 = \frac{Z_g - Z_c}{Z_g + Z_c} \;\text{ and }\; \rho_2 = \frac{Z_c - Z_g}{Z_g + Z_c} \tag{16}$$

where Z_g and Z_c are the characteristic impedance of the PSW with and without an added dielectric medium, respectively. The transmission factors τ_i in (15) is obtained as $\tau_i = 1 - \rho_i^2$.

Finally, the matrix **A** can be constructed for all the incident fields as shown in (8) using the values of the reflection and transmission coefficients at each junction. The incident field E_s is utilized to determine the excited ports. Thus, by solving (8), the incident field values at all the junctions are estimated. In order to calculate the output field from the port, the relationship between the input and the output field at each junction given in (4) is utilized. Thus, the final output field can be obtained as follows

$$E_o = \mathbf{B}E_i = \mathbf{B}\mathbf{A}^{-1}E_s \tag{17}$$

where the matrix **B** is a block diagonal matrix and given as

$$\mathbf{B} = \begin{pmatrix} S_1 & & & \\ & \ddots & & \\ & & S_n & \\ & & & S_N \end{pmatrix}, \tag{18}$$

where

$$S_n = \begin{pmatrix} r_1 & t_1^l & t_1^t & t_1^r \\ t_2^r & r_2 & t_2^l & t_2^t \\ t_3^t & t_3^r & r_3 & t_3^l \\ t_4^l & t_4^t & t_4^r & r_4 \end{pmatrix}_n \tag{19}$$

Thus, the system of equations in (17) can be solved efficiently by placing the junction scattering matrix in (19) for each junction. This process is homogenous for all the inner junctions. Then the boundary junctions and junctions with special connections are treated individually as explained hereafter. The size of the system of equations is limited by the number of junctions, which allow for very fast solution compared to the FDTD method.

The proposed approach is also solved numerically similar to the FDTD method [23] and the conventional TLM techniques [27]. However, the main difference in our case is the unit cell of each method. In any conventional full wave numerical method the unit cell is much smaller than wavelength. In particular, the cell size for plasmonic waveguides is usually on the order of a few nanometers to provide the required accuracy. This results in thousands of cells if not much more. In our approach, on the other hand, the unit cells are the junction. This results in few tens of cells only. Thus, our approach is far more efficient as it only deals with few junctions only and hence it involves at least 2–3 orders of magnitude less cells in comparison to any conventional full wave method.

4. Device performance and sensitivity analysis

Calculating the sensitivity of the response for the network with respect to all the design variables is essential for gauging the structure tolerance and yield. It also allows for using gradient-based optimization technique to obtain the required specifications. However, full electromagnetic numerical solvers do not provide such information. Special approaches such as adjoint variable method can be applied to get the sensitivity information in an efficient manner [28–31]. However, this sensitivity information requires FDTD simulations at each design point. On the other hand, the analytical closed form approach in [15, 17] allow for exact calculations to obtain the sensitivity by direct derivative of the response of the network. The semi-analytical approach given in section 3 does not directly provide sensitivity information. However, the sensitivity information can be obtained in an efficient manner as will be described here.

In order to obtain the sensitivity of any function $f\left(E_o\right)$ calculated from the field response such as the transmitted power, reflected power and insertion loss, a finite difference scheme is usually utilized. However, for large number of design parameters, this approach is inefficient as it requires large number of additional simulations. For example, for N design parameters, $2N$ extra FDTD simulations are required to obtain the sensitivity information with respect to all the design parameters using central finite difference scheme. In this section, we demonstrate an efficient approach to obtain the sensitivity information without the need of running the extra simulations.

We start by differentiating the function $f\left(E_o\right)$ with respect to the design variable x_p and use the chain rule as given below

$$\frac{\partial f\left(E_o\right)}{\partial x_p} = \frac{\partial f\left(E_o\right)}{\partial E_o}\frac{\partial E_o}{\partial x_p} \tag{20}$$

By substituting (17) into (20), we obtain

$$\frac{\partial f}{\partial x_p} = \frac{\partial f}{\partial E_o}\frac{\partial\left(\mathbf{B}\mathbf{A}^{-1}E_s\right)}{\partial x_p} \tag{21}$$

By differentiating we obtain

$$\frac{\partial f}{\partial x_p} = \frac{\partial f}{\partial E_o}\left(\frac{\partial(\mathbf{B})}{\partial x_p}\mathbf{A}^{-1}E_s - \mathbf{B}\mathbf{A}^{-1}\frac{\partial(\mathbf{A})}{\partial x_p}\mathbf{A}^{-1}E_s\right) \tag{22}$$

In (22), the source field is assumed independent for the objective function $f\left(E_o\right)$. Thus, it can be rewritten as

$$\frac{\partial f}{\partial x_p} = \frac{\partial f}{\partial E_o}\left(\frac{\partial(\mathbf{B})}{\partial x_p}E_i - \mathbf{B}\mathbf{A}^{-1}\widehat{E_i}\right) \tag{23}$$

where

$$\widehat{E_i} = \frac{\partial(\mathbf{A})}{\partial x_p}E_i \tag{24}$$

The terms E_i and $\mathbf{A}^{-1}$ are obtained through solving the original system given in the system in (8) and (17). Thus, the only remaining terms required to evaluate the sensitivity expression in (23) are the system derivatives $\partial(\mathbf{B})/\partial x_p$ and $\partial(\mathbf{A})/\partial x_p$. These derivatives can be obtained analytically by differentiating the elements of these matrices with respect to each design parameters. An approximate derivative of the system matrices can be also obtained

$$\frac{\partial(\mathbf{A})}{\partial x_p} \approx \frac{\mathbf{A}\left(x_p + \Delta x_p\right) - \mathbf{A}(x_p)}{\Delta x_p} \tag{25}$$

The calculated derivative of the system matrices is highly sparse matrices and have nonzero values only at the element corresponds to perturbed parameters. Once the derivative matrices are obtained the sensitivity expression given in (23) can be calculated. It worth noting that the term $\mathbf{A}^{-1}$ is readily obtained from the solution of the original problem (17).

5. Application examples

In this section, various designs utilizing networks of PSWs are examined and their performance discussed and compared to the one obtained from FDTD. These examples are chosen in part because their analysis using FDTD would require

significant computational resources. On the other hand these examples are also chosen to have a size and complexity such that using the previously developed techniques to obtain closed form expressions would yield complex equations that would provide less insight into their behavior. As such, we chose examples where the analysis technique used in this work would be optimum approach to analyze them.

5.1. Dual bandstop filter design using 3 × 3 network

In this example, 3×3 network is exploited to design an interference based bandstop filter with dual stop wavelengths. This structure contains nine junctions and the possibility to obtain a closed form expression requires analysis of the field travelling through each of the nine junctions for each port excitation. This process is extremely inefficient. On the other hand, FDTD simulation of this structure would require a few hours to run and hence would not be a suitable technique for optimizing such network.

Due to the use of symmetric junctions, the implementation of the proposed approach is straightforward and a generalized junction matrix that is suitable for all the junctions is calculated using (4) once for all the junctions. The excitation vector contains only two nonzero elements with value of 1.0 corresponding to the excitation of the two input ports as shown in figure 9. The constructed system matrix dimensions are 36×36. Once (17) is solved for this system, the response at all the output port is readily available. The structured network is optimized such that, the filter response is a bandstop filter with tuneable stopband center wavelength at 1500 nm and 1550 nm. The dimensions of the network are $l_x = l_y = 700$ nm, the width of the PSW, W_x and W_y are equal and taken to be 250 nm. The input and output ports are marked in figure 9. The transmitted power is shown in figure 10. The results obtained using our model are compared with its FDTD [23] counterparts in figure 10. Good agreement is obtained between both, which validates the accuracy of our model. The output from port 2 and port 3 are similar with stopband center wavelength of 1500 nm. In addition, the output from port 1 and port 4 are similar with stopband center wavelength of 1550 nm. The performance of this filter is of great interest as it allows for multiple outputs with similar response and also allows for different resonance wavelengths from different sides. The filter exhibits very high extension ratio more than 30 dB as shown in figure 10. The shift in the resonance wavelength at different ports can be attributed to the presence of concatenated coupled resonance paths inside the network. The possibility to obtain multiple functionalities from a structure with a foot print of $2\,\mu m\times2\,\mu m$ is unique achievement of this PSW based structures. The ability to obtain same functionality using dielectric resonators with the same dimension scale suffers from high radiation losses [15].

The sensitivity of the transmission with respect to all the design parameters is calculated using the procedure given in section 4. The results obtained using our approach match closely with those calculated using the finite difference scheme which is applied directly on the behavior obtained from the FDTD calculations. For example, the sensitivity of

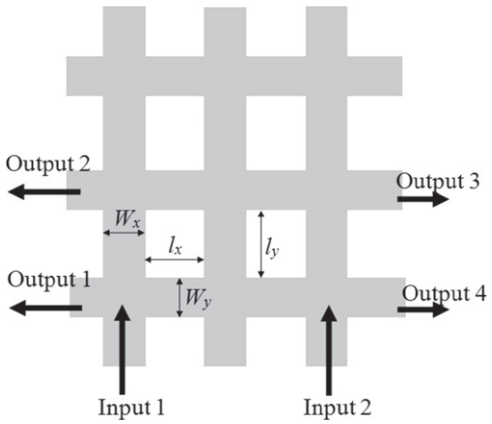

Figure 9. Schematic diagram of the dual band filter using 3×3 plasmonic network shown in section 5.1.

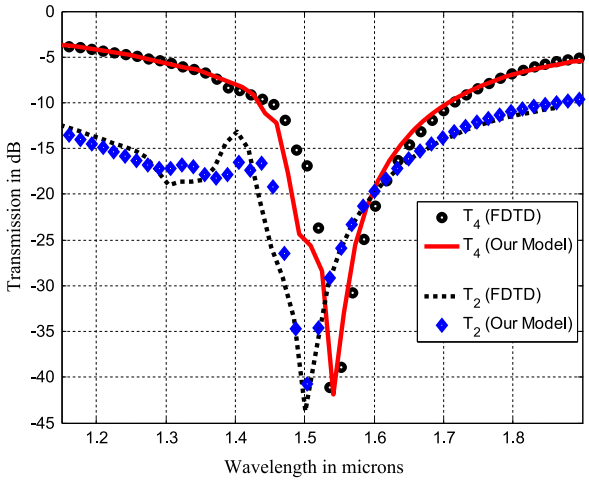

Figure 10. The normalized power transmission of the bandstop dual band filter using 3×3 plasmonic network shown in section 5.1.

the transmitted power from port 2 with respect to the change in the width of the vertical slot line W_{x1} is calculated and compared with those obtained using FDTD with good match as shown in figure 11. The information extracted from this sensitivity can be utilized to understand the impact of any of the design parameters on the performance of the network. It can also be exploited to maximize or minimize the response with respect to the change in any of the design parameters. For example, in figure 11 it is clear that the transmitted power has very week dependence on the change of W_{x1} around the wavelength band from 1450 nm to 1550 nm. This is an attractive attribute that enables one to manage the fabrication tolerances. On the other hand, the same figure also show high sensitivity of the same parameter around wavelength of 1400 nm which suggests that operating in this band requires very low tolerance with respect to the network parameters. Thus, the sensitivity analysis demonstrates that the proposed structure has good tolerance to the structure dimensions within the proposed working bandwidth.

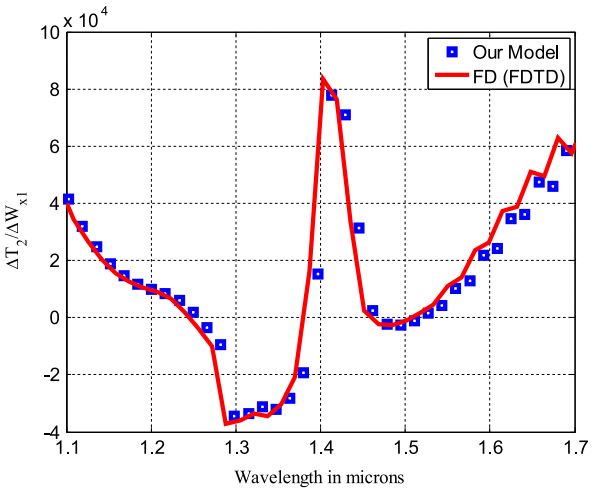

Figure 11. The sensitivity of the transmission with respect to W_{x1} of the bandpass dual band filter using 3×3 plasmonic network shown in section 5.1.

5.2. Dual band all optically controlled modulator using subwavelength 5 × 5 network

In this example, the plasmonic network shown in figure 12 is utilized to design all optically controlled dual band modulators. The functionality of the structure is based on controlling the transmitted power from the output port using one or two inputs. The functionality is obtained using our modelling approach by using a simple optimization algorithm that maximizes the extinction ratio at the output ports in the case of only input 1 is on, versus the case of both inputs 1 and 2 are on. This algorithm has been successfully implemented to achieve the required functionality at dual wavelength bands (1.55 μm and 1.75 μm) simultaneously using the same structure at the same output port.

The optimal design parameters of this network are summarized as follows: the arm length ($l_x = l_y$) of the network is calculated to be 460 nm only, which is subwavelength and avoid any interference effects in the arm. The slot widths are 50 nm for all the arms in the network. The output power due to the excitation of port 1 is T_{o1} and is shown in figure 13. The output from the same port due to the excitation of both input ports is T_{o2} and also shown in the same figure. The results agree well with those obtained from the FDTD over the entire band of interest.

The modulation is obtained by controlling the power in input port 2. If port 2 is excited in phase with port 1: (a) the output power will be minimized at the output port around the 1550 nm with an extinction ratio of more than 30 dB, (b) the output power is maximized at 1750 nm with an extinction ratio of 15 dB. To verify this performance, the optimal structure is also simulated using FDTD as shown in figure 13. The optimization process takes only few minutes using our approach. On the other hand, the FDTD simulation which is only used for verification require more than 12 h.

The sensitivity of the transmitted power from output port with respect to the change in the width of the vertical slot line W_{x1} is also calculated and compared with those obtained using FDTD with good match as shown in figure 14. This

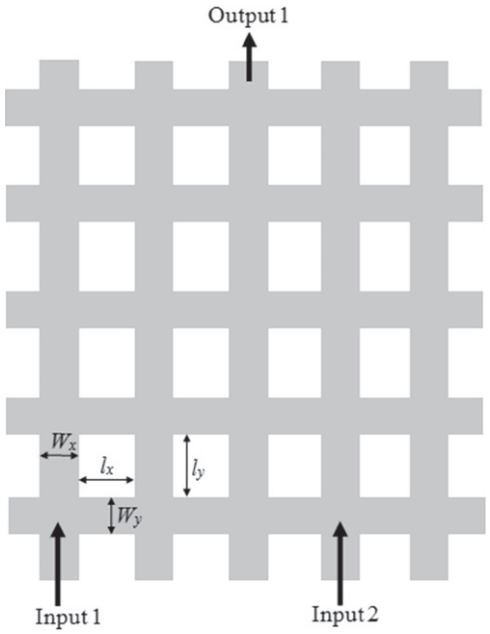

Figure 12. Schematic diagram of all optical modulator using 5×5 network shown in section 5.2.

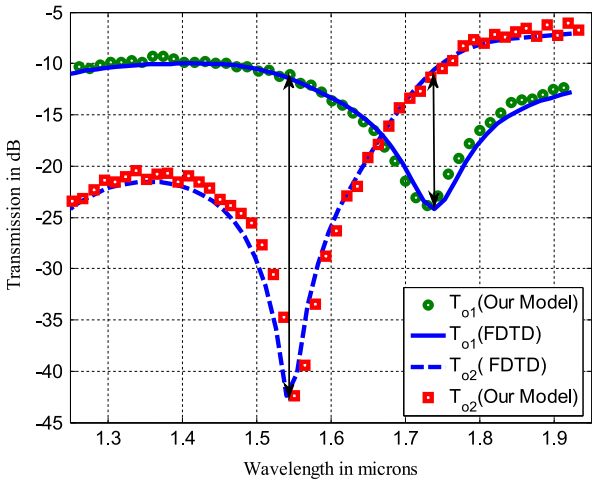

Figure 13. The normalized transmission response of output due to the excitation of the input ports of the optical modulator shown in section 5.2.

sensitivity analysis shows that the transmission has weak dependence on the around W_{x1} in the range between 1600–1700 nm. Also it shows that the transmission has constant change rate in the range from 1800–1900 nm.

5.3. Wideband filter using irregular network

In order to demonstrate the generality of our approach, an irregular network is designed and optimized to have a wideband filter response. The network architecture is shown in figure 15. In this architecture, different junction types and connections are exploited to obtain the required response. The dimensions of the proposed structure are given as $L_1 = 0.62\,\mu$m, $W_1 = 0.15\,\mu$m, $W_2 = 0.07\,\mu$m, $W_3 = W_4 = W_5 = 0.1\,\mu$m, $L_2 = 0.67\,\mu$m, $L_3 = 0.56\,\mu$m, $L_5 = 0.63\,\mu$m, and $\theta_1 = \theta_2 = \theta_3 = \theta_4 = 30°$.

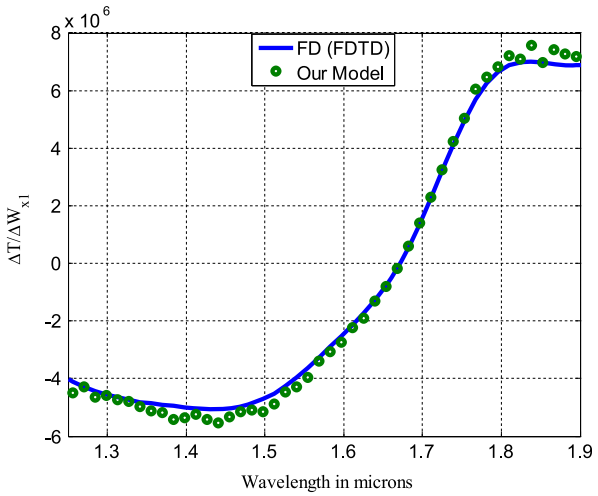

Figure 14. The sensitivity of the transmission of the optical using 5×5 plasmonic network shown in section 5.2.

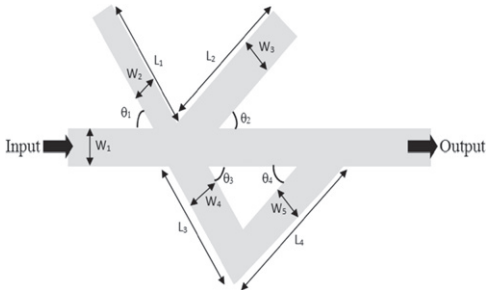

Figure 15. Schematic diagram of optical filter using asymmetric network shown in section 5.3.

In this example, the proposed modelling approach is exploited to model a network with a five-port junction. The equations that describe each junction are modified based on the number of ports. Thus, the junction equations in (4) have been modified accordingly for each case. For example, five equations are written for the transmission through the five-ports junction. For the angled junction the reflection is assumed be negligible and a transmission of 98% is assumed based on the sharp junction transmission properties [13]. The 2D FDTD simulations show that for angle smaller than ~30, the amount of power coupled to the angled arm starts to deviate from those of orthogonal angle without much increase in the reflection power. The reflection from real metal given in (12) is utilized to update the stub equations using (11). The final response is obtained after solving the constructed system of equations as the one in (17). The obtained response using our approach is shown in figure 16. As can be seen in this figure a good agreement between our approach and FDTD is also obtained.

6. Conclusion

A general approach for modelling any network configuration designed using PSW is discussed and analyzed. The approach is accurate and efficient compared with FDTD. The model is

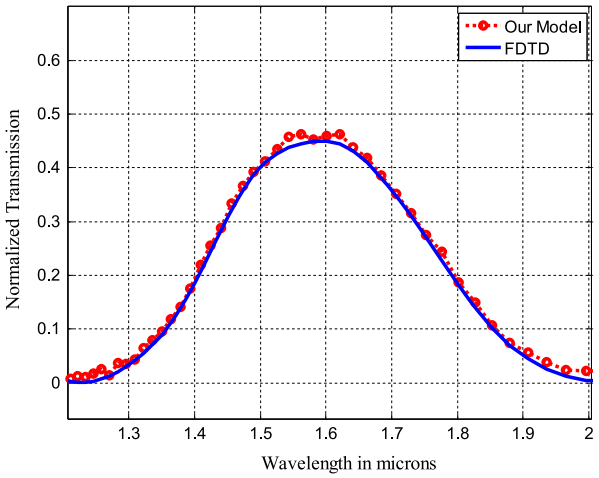

Figure 16. The filter response of the irregular network using both our approach and FDTD shown in section 5.3.

numerical and utilizes simple impedance models to represent the junctions for each junction, which make up the grid nodes of the numerical simulations. This drastically reduces the computational resources needed in comparison to FDTD, which requires sub-wavelength grid. An efficient approach for sensitivity analysis is also discussed. Various PSW network structures with useful functions have been examined using this modeling approach.

References

[1] Homola J 2003 Present and future of surface plasmon resonance biosensors *Anal. Bioanal. Chem.* **377** 528–39
[2] Swillam M A and Helmy A S 2010 Analysis and applications of 3D rectangular metallic waveguides *Opt. Express* **18** 19831–43
[3] Ozbay E 2006 Plasmonics: merging photonics and electronics at nanoscale dimensions *Science* **311** 189–93
[4] Maier S A 2006 Plasmonic field enhancement and SERS in the effective mode volume picture *Opt. Express* **14** 1957–64
[5] Berini P 2008 Bulk and surface sensitivity of surface plasmon waveguides *New J. Phys.* **10** 105010
[6] Dionne J A, Sweatlock L A and Atwater H A 2006 Plasmonic slot waveguides: towards chip-scale propagation with subwavelength-scale localization *Phys. Rev.* B **73** 035407
[7] Zia R, Schuller J A, Chandran A and Brongersma M L 2006 Plasmonics: the next chip-scale technology *Mater. Today* **9** 20–7
[8] Guo Y, Yan L, Pan W, Luo B, Wen K, Guo Z, Li H and Luo X 2011 A plasmonic splitter based on slot cavities *Opt. Express* **19** 13831–8
[9] Hu F, Yi H and Zhou Z 2011 Wavelength demultiplexing structure based on arrayed plasmonic slot cavities *Opt. Lett.* **36** 1500–2
[10] Hu F and Zhou Z 2005 Wavelength filtering and demultiplexing structure based on aperture-coupled plasmonic slot cavities *Opt. Soc. Am.* B **28** 2518–23
[11] Lau B, Swillam M A and Helmy A S 2010 Hybrid orthogonal junctions: wideband plasmonic slot-silicon waveguide couplers *Opt. Express* **18** 27048–59
[12] Lin C, Wong H M K, Lau B, Swillam M A and Helmy A S 2012 Efficient broadband energy transfer via momentum matching at hybrid guided-wave junctions *Appl. Phys. Lett.* **101** 123115

[13] Veronis G and Fan S 2005 Bends and splitters in metal–dielectric–metal subwavelength plasmonic waveguides *Appl. Phys. Lett.* **87** 131102
[14] Swillam M A and Helmy A S 2011 Filter response of feedback plasmonic junctions *Integrated Photonics Research, Silicon and Nanophotonics, OSA Technical Digest (CD)* (Washington DC: Optical Society of America)
[15] Swillam M A and Helmy A S 2012 Feedback effects in plasmonic slot waveguides examined using a closed-form model *Photonics Technol. Lett.* **24** 497–9
[16] Feigenbaum E and Atwater H 2010 Resonant guided wave networks *Phys. Rev. Lett.* **104** 147402
[17] Lin C, Swillam M A and Helmy A S 2012 Analytical model for metal–insulator–metal mesh waveguide architectures *J. Opt. Soc. Am.* B **29** 3157–69
[18] Han Z and Bozhevolnyi S 2013 Radiation guiding with surface plasmon polaritons *Rep. Prog. Phys.* **76** 016402
[19] Feigenbaum E and Orenstein M 2007 Perfect 4-way splitting in nano plasmonic X-junctions *Opt. Express* **15** 17948–53
[20] Lin X and Huang X 2008 Tooth-shaped plasmonic waveguide filters with nanometeric sizes *Opt. Lett.* **33** 2874–6
[21] Nejati H and Beirami A 2012 Theoretical analysis of the characteristic impedance in metal–insulator–metal plasmonic transmission lines *Opt. Lett.* **37** 1050–2
[22] Palik E D 1985 *Handbook of Optical Constants of Solids* (Florida: Academic)
[23] Lumerical, "Multicoefficient Material Modelling in FDTD; www.lumerical.com
[24] David D M 2012 *Microwave Engineering* 4th edn (New York: Willey)
[25] Kocabas S E, Veronis G, Miller D A B and Fan S 2008 Transmission line and equivalent circuit models for plasmonic waveguide components *IEEE J. Sel. Top. Quantum Electron.* **14** 1462–72
[26] Pannipitiya A, Rukhlenko I D, Premaratne M, Hattori H T and Agrawal G P 2010 Improved transmission model for metal–dielectric–metal plasmonic waveguides with stub structure *Opt. Express* **18** 6191–204
[27] Hoefer W J R 1985 The transmission line matrix method - Theory and applications *IEEE Trans. Microw. Theory Tech.* **33** 882–93
[28] Swillam M A, Bakr M H and Li X 2008 Full wave sensitivity analysis of guided wave structures using FDTD *J. Electromagn. Waves Appl.* **22** 2135–45
[29] Swillam M A, Bakr M H and Li X 2007 Accurate sensitivity analysis of photonic devices exploiting the finite-difference time-domain central adjoint variable method *J. Appl. Opt.* **46** 1492–9
[30] Swillam M A, Bakr M H, Nikolova N K and Li X 2007 Adjoint sensitivity analysis of dielectric discontinuities using FDTD *J. Electromagn.* **27** 123–40
[31] Swillam M A, Gohary R H, Bakr M H and Li X 2009 Efficient approach for sensitivity analysis of lossy and leaky structures using FDTD *J. Prog. Electromagn. Res.* **94** 197–212